Thomas Veltzke, Fabian Pille, Jorg Thöming

Delayed binary and multicomponent gas diffusion in conical tubes

Journal Article	as:	peer-reviewed accepted version (Postprint)
DOI of this document*(secondary publication):		https://doi.org/10.26092/elib/2447
Publication date of this document:		07/09/2023

* for better findability or for reliable citation

Recommended Citation (primary publication/Version of Record) incl. DOI:

Thomas Veltzke, Fabian Pille, Jorg Thöming,
Delayed binary and multicomponent gas diffusion in conical tubes,
Chemical Engineering Science, Volume 148, 2016, Pages 93-107, ISSN 0009-2509,
https://doi.org/10.1016/j.ces.2016.03.029

Delayed binary and multicomponent gas diffusion in conical tubes

Thomas Veltzke*, Fabian Pille, Jorg Thöming

Center for Environmental Research and Sustainable Technology (UFT), University of Bremen, Leobener Str. 1, 28359 Bremen, Germany

HIGHLIGHTS

- Mass transport is delayed by the conical geometry of tubes representing pores.
- Delay effect increases with ratio of inlet to outlet tube radius.
- Development and mathematical description of a novel steady-state diffusion cell.
- Comparability to the transient two-bulb-diffusion-cell.

GRAPHICAL ABSTRACT

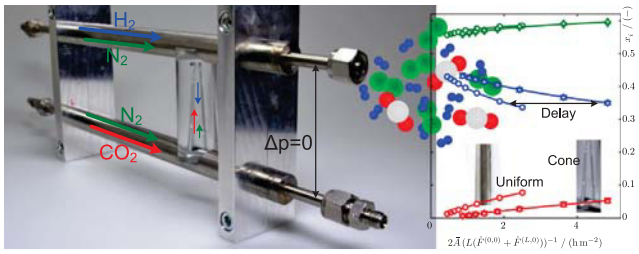

ARTICLE INFO

Article history:
Received 23 November 2015
Received in revised form
24 January 2016
Accepted 20 March 2016
Available online 31 March 2016

Keywords:
Transport limitation in catalysis
Steady-state multicomponent diffusion
Novel diffusion experiment
Conical test tube
Transport delay

ABSTRACT

Catalyst pores are typically non-uniform along their longitudinal axis, and the transport of gaseous reactants and products takes place in a somehow tapered confinement. In a previous study we observed a diffusion delay in single tapered pores by means of a transient two-bulb-diffusion-cell (Veltzke et al., 2015). Processes in heterogeneous catalysis, however, are typically operated under steady state conditions. Hence also the diffusion processes are non-transient and reactant species are permanently consumed while product species steadily emerge. To mimic steady-state multicomponent diffusion in a cone, we developed a novel two-pipe-diffusion-cell and described the mass transport by an analytical model.

Here we can show that the delay effect, which is caused by volumetric changes in longitudinal direction, also exists for steady-state binary and multicomponent diffusion. It is experimentally confirmed that the diffusion hindrance increases with conicity of the test tube. Also the results are transferable to those of the transient two-bulb-diffusion-cell. The measurement of steady-state experiments, however, is much faster.

1. Introduction

The relevance of gaseous diffusion from the macroscale in reactors to the microscale in catalyst pores is most substantial for the overall yield and performance in heterogeneous catalysis. Due to the unique properties of microscale pores that arise from their small size and large specific surface area, high reaction rates per unit volume are given (Wang and Coppens, 2008). In terms of mass transport limitation, the transport mechanisms of reactants to the catalytically active site and those of the products from the active site of the catalyst determine the amount of required catalyst. For this reason, it is the objective in research to improve the mass transport without decreasing the specific surface area.

A crucial parameter for the mass transport is the pore geometry. Some studies about the influence of the geometry on gas diffusion are given in literature (Dogu and Dogu, 1980; Loewenberg, 1994; Dogu, 1998; Graur et al., 2015). Recently, an experimental and analytical study on transient diffusion of an ideal ternary mixture was presented by the authors where it was shown that the mass transport is slower in a conical tube compared to a uniform one with identical average cross section (Veltzke et al., 2015). Diffusion processes in heterogeneous catalysis, however, are

* Corresponding author.
E-mail addresses: tveltzke@uni-bremen.de (T. Veltzke), fabian.pille@web.de (F. Pille), thoeming@uni-bremen.de (J. Thöming).

http://dx.doi.org/10.1016/j.ces.2016.03.029

typically non-transient since reactant species are permanently consumed while product species steadily emerge. Mass transport studies involving the influence of pore geometry obtained on transient considerations cannot be transferred to the more realistic steady-state conditions arbitrarily. The aim of the present paper, hence, is to study ideal binary and ternary diffusion through an idealized single pore under stationary conditions.

To obtain steady-state diffusion we designed an experimental setup consisting of two pipes perfused steadily by different gases (gas mixtures) that are orthogonally connected to a test tube (either uniform or conical). A mathematical description of this novel gas diffusion cell is derived in order to predict the steady-state binary and multicomponent diffusion process. A further aspect of the model is the consideration of the fluid velocity by the Reynolds number which is used as a weighting factor to iteratively determine the concentrations of the outflowing gas mixture streams. The numerical solution of this model allows us the prediction of the concentrations of gases leaving the system. Further, the effect of the conicity of test tubes is investigated experimentally. We can show that the conicity of the test tubes leads to a delay of the transport which confirms the findings in Veltzke et al. (2015).

The first part of this paper is focused on the mathematical description of the considered experiment and the model development. Afterwards, the experimental setup and procedure are described and the experimental results are compared to the theoretical ones. The last chapter concludes the findings.

2. Model development and analysis

Independently of the diffusion process being transient or steady-state, the mathematical description is distinguished by the number of involved gas species. The common approach to describe binary molecular diffusion is Fick's law (Fick, 1855) which defines that the molar flux is proportional to its concentration gradient and directed against it. For a ternary gas mixture, however, multicomponent effects arise that can be explained by the Maxwell-Stefan equations while Fick's law fails (Duncan and Toor, 1962).

2.1. Problem statement

To obtain stationary conditions of concentrations on each side of a long test tube with alongside variable cross section, two pipes creepingly perfused with different gas mixtures with n species i are orthogonally connected to each end of the tube. The pipes can be interpreted as infinitely large gas reservoirs. The setup is deduced from the experimental approaches in literature (Taylor and Krishna, 1993; Wicke and Kallenbach, 1941; Soukup et al., 2008) and illustrated in Fig. 1 as an abstraction of an idealized catalyst pore where the concentrations at each end of the tube are constant. This means the consideration of stationary conditions from the reactant-rich end (mix 1) to the product-rich end (mix 2) of the pore.

The first longitudinal coordinate z is defined as that one within the tube with its origin in the system of mix 1 at $z = 0$. According to Fig. 1, the length of the tube is L_{tube} and the varying cross section is $A_{\text{tube}}(z)$. Correspondingly, the upper system of mix 1 at $z = 0$ is indicated by the first superscript (0) and the lower system of mix 2 at $z = L_{\text{tube}}$ by the first superscript (L). Consequently, the diameter of the tube at the mix 1 system is $d_{\text{tube}}^{(0)}$ whereas $d_{\text{tube}}^{(L)}$ is that one of the mix 2 system. The second longitudinal coordinate is defined as the flow direction within the pipes with the origin at the inlet into the system of mix 1 at $y_0=0$ and with that one of mix 2 at $y_L=0$. Corresponding to the z-direction, the inlet of a mix system is indicated by the second superscript (0) and the outlet by the second superscript $d^{(0)}$ and $d^{(L)}$, respectively. The diameters of both pipes are identical.

In the following, we derive the species balance in the pipes in the first part, followed by a species balance in the tube. In the last section, we bring both parts together to obtain the model solution.

2.2. Species balance in the pipes

The integral species balance over the mixing zone of pipe A at $z = 0$ (indicated by superscript index 0) in Fig. 1b writes

$$\frac{dN_i^{(0)}}{dt} = n_i^{(0,0)} A_{\text{pipe}} - n_i^{\left(0,d^{(0)}\right)} A_{\text{pipe}} - J_i^{(0)} A_{\text{tube}}^{(0)} \tag{1}$$

and in pipe B at $z = L_{\text{tube}}$ (indicated by superscript index L)

$$\frac{dN_i^{(L)}}{dt} = n_i^{(L,0)} A_{\text{pipe}} - n_i^{\left(L,d^{(L)}\right)} A_{\text{pipe}} + J_i^{(L)} A_{\text{tube}}^{(L)}, \tag{2}$$

where dN_i/dt is the temporal change of the amount of species i, n_i is the convective flux in the pipes and J_i is the diffusive flux of species i in the tube counted positive in positive z-direction.

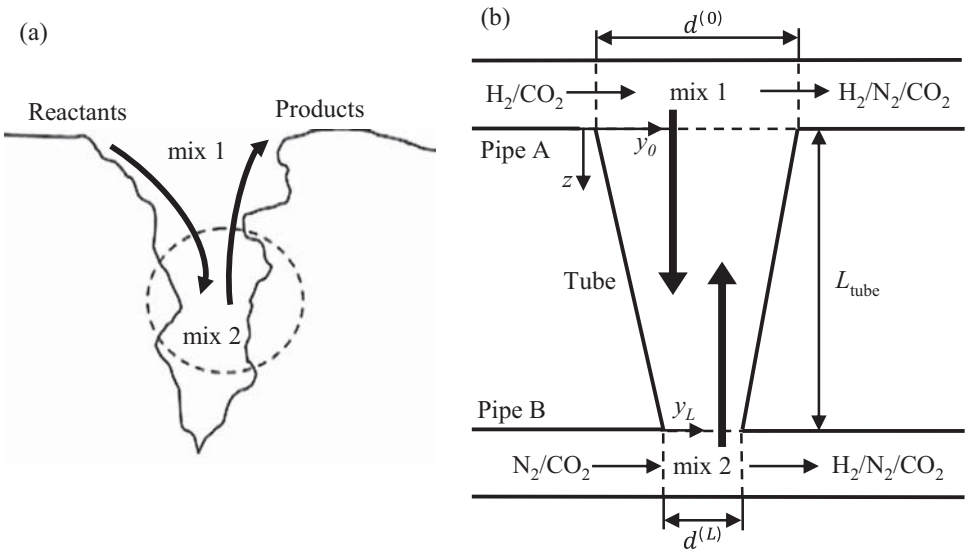

Fig. 1. Abstraction of an idealized catalyst pore to the stationary two-pipe-diffusion experiment. (a) Reactants permanently enter the pore and react to products that steadily leave the pore (Fick, 1855). (b) The abstracted model leads to the stationary diffusion experiment with a conical tube under constant concentration conditions at its ends.

Indexing n_i with superscript $(L,d^{(L)})$, for instance, refers to the convective flux in pipe B at position $y_L=d^{(L)}$ according to Fig. 1b. A_{pipe} defines the constant and identical cross sections of both pipes and A_{tube} is the cross section of the tube at both particular positions $z=0$ and $z=L_{\text{tube}}$, respectively. It is assumed that the gas mixtures in both mixing zones are perfectly mixed and that the convective as well as the diffusive fluxes are homogeneously distributed over the cross sections of the pipes and the tube. Further, we assume isobaric conditions due to the aperture of both pipes to an infinitely large reservoir (i.e., the atmosphere), low Reynolds numbers *Re* (creeping flow), low Mach numbers *Ma* (subsonic flow) and low Knudsen numbers *Kn* (continuum regime). Those dimensionless numbers are defined as

$$Re=\frac{ud}{\upsilon},\ Ma=\frac{u}{u_0},\ Kn=\frac{\lambda}{d} \tag{3}$$

with u being the gas velocity, d the pipe/tube diameter, υ the kinematic viscosity of the gas, u_0 the speed of sound, and λ the mean free path. Assuming the steady-state, isothermal and non-reacting conditions and a constant cross section of the pipes, Eqs. (1) and (2) result in

$$0=\left(n_i^{(0,0)}-n_i^{\left(0,d^{(0)}\right)}\right)A_{\text{pipe}}-J_i^{(0)}A_{\text{tube}}^{(0)} \tag{4}$$

and

$$0=\left(n_i^{(L,0)}-n_i^{\left(L,d^{(L)}\right)}\right)A_{\text{pipe}}+J_i^{(L)}A_{\text{tube}}^{(L)}. \tag{5}$$

In the following, we focus on pipe A (Fig. 1b; first index 0) since the derivation of pipe B (first index L) is analogous and therefore not stated here explicitly.

The change of the convective flux of each species i in the mixing zone of pipe A is described by the linear extrapolation

$$n_i^{\left(0,d^{(0)}\right)}=n_i^{(0,0)}+\frac{dn_i^{(0)}}{dy_0}y_0 \text{ with } 0<y_0<d_{\text{tube}}^{(0)}. \tag{6}$$

Here it is worth to note that this assumption is made for reasons of simplification and follows up the assumption of the diffusive fluxes being homogeneously distributed over the cross section of the tube. Applying Eq. (6) to Eq. (4) and dividing by A_{pipe} lead to

$$\frac{dn_i^{(0)}}{dy_0}=-J_i^{(0)}\frac{A_{\text{tube}}^{(0)}}{A_{\text{pipe}}\,y_0}. \tag{7}$$

Integration of Eq. (7) yields

$$n_i^{\left(0,d^{(0)}\right)}=n_i^{(0,0)}-J_i^{(0)}\frac{A_{\text{tube}}^{(0)}}{A_{\text{pipe}}\,y_0}\int_0^{y_0}dy_0=n_i^{(0,0)}-J_i^{(0)}\frac{A_{\text{tube}}^{(0)}}{A_{\text{pipe}}}. \tag{8}$$

Because $A_{\text{tube}}^{(0)}$ is independent of the y_0-direction and A_{pipe} is constant, $A_{\text{tube}}^{(0)}$ and A_{pipe} can be taken as prefactors.

The composition gradient is computed by the Maxwell-Stefan equation as

$$\frac{dx_i^{(0)}}{dz}=-\sum_{\substack{j=1\\ j\neq i}}^{n}\frac{x_i^{(0)}x_j^{(0)}}{Đ_{ij}}(u_i-u_j)=\sum_{\substack{j=1\\ j\neq i}}^{n}\frac{x_i^{(0)}J_j^{(0)}-x_j^{(0)}J_i^{(0)}}{c_t Đ_{ij}}. \tag{9}$$

Here c_t is the total molar concentration in both pipes and $c_t=p/(R_0T)$ follows the ideal gas law with p as the pressure, T as the temperature and R_0 as the universal gas constant. x_i and x_j are the molar fractions and (u_i-u_j) is the relative velocity between both species i and j, respectively. $Đ_{ij}$ are the Maxwell-Stefan binary diffusivities estimated by the Chapman-Enskog kinetic theory and possess the physical significance as an inverse drag coefficient (Taylor and Krishna, 1993).

In a binary gas mixture, the flux of only one species is measured and the molar flux of the other species is assumed to be equal and opposite. Hence, the total diffusive molar flux summed over n components is zero, given by (Taylor and Krishna, 1993)

$$\sum_{i=1}^{n}J_i^{(0)}=0, \tag{10}$$

which in the following is referred to as *equimolar* diffusion. Consequently, the amount of species reduces from n to $n-1$ and the MSE according to Eq. (9) can be written in an explicit, Fickian form. The equimolar diffusive flux of species i, hence, *is* given by

$$J_i^{\text{eqmol},(0)}=J_i^{(0)}=-c_t\sum_{j=1}^{n-1}D_{ij}\frac{dx_j^{(0)}}{dz}, \tag{11}$$

when keeping in mind that the sum of all species must be unity (Veltzke et al., 2015)

$$\sum_{i=1}^{n}x_i^{(0)}=1 \text{ or } \sum_{i=1}^{n}\frac{dx_i^{(0)}}{dz}=0. \tag{12}$$

(Eqs. (11) and 12) show that only $n-1$ gradients are independent from each other. The matrix of multicomponent diffusivities D is related to the Maxwell–Stefan diffusivities $Đ_{ij}$ for an ideal gas by (Taylor and Krishna, 1993)

$$[D]=[B]^{-1}, \tag{13}$$

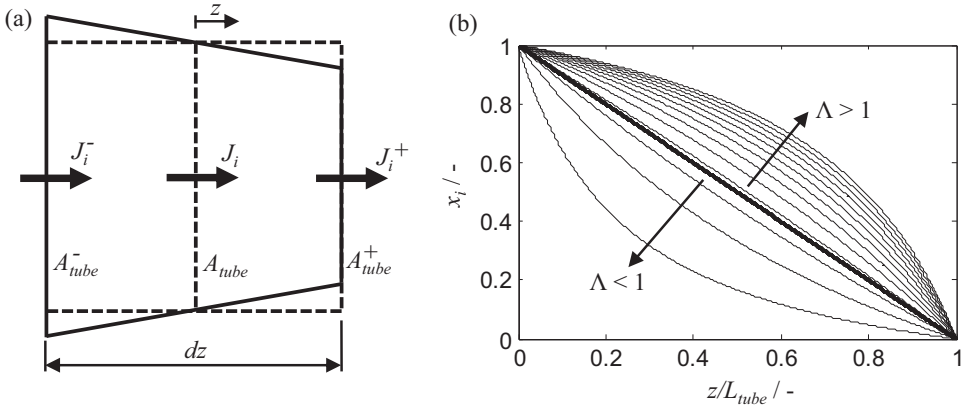

Fig. 2. (a) Infinitesimal part of a conical tube (solid lines) with the identical average cross section A_{tube} as a uniform one (dashed lines). (b) Qualitative concentration profiles over the tube length as a function of the ratio of A_{tube}^- to A_{tube}^+.

with

$$B_{ii} = \frac{x_i}{Đ_{in}} + \sum_{\substack{j=1 \\ j\neq i}}^{n} \frac{x_j}{Đ_{ij}},\ B_{ij} = -x_i\left(\frac{1}{Đ_{ij}} - \frac{1}{Đ_{in}}\right), \tag{14}$$

using equilibrium values for x_i and x_j. Although $Đ_{ij} \geq 0$ for ideal gases, the multicomponent diffusivities in Eq. (11) can be negative due to multicomponent effects and depend on the molar fractions x_i and x_j, respectively. Bird et al., (2007), Taylor and Krishna (1993), Fahien (1983) and Cussler (1997) regard an equimolar countercurrent diffusive transport by the MSE, Eq. (11). The assumption of equimolar counter-current diffusion is commonly used for chemical engineering applications (Farr, 1993).

2.3. Duct species balance

To obtain the concentration gradients at the inlets of the tube, an infinitesimal part of a cone is considered in Fig. 2a, following Fick (1855).

The derivation of the concentration gradient is presented for the quasi-stationary case in detail in Veltzke et al. (2015). The species balance for the infinitesimal tube section is obtained by using Taylor series to describe the influxes and outfluxes. Assumption of stationary conditions and applying the chain rule yield

$$\frac{d}{dz}(J_i A_{\text{tube}})dz = 0,\ \frac{dJ_i}{dz} + J_i \frac{1}{A_{\text{tube}}}\frac{dA_{\text{tube}}}{dz} = 0. \tag{15}$$

Here, we regard the diffusive flux J_i. Using diffusion experiments in closed diffusion cells as continuum processes, the molar diffusion rates of the components are equal for a binary mixture and equimolar countercurrent transport mostly occurs (Evans et al., 1961). However, under isobaric conditions in open systems, different assumptions for the diffusive transport models are presented in literature as shown in the following.

In a binary gas mixture consisting of species with significantly different molecular masses and a composition gradient, a net molecular flux from the side of light molecules to the side of heavier ones at uniform total pressure and temperature leads to an accumulation on the side of the "heavier" gas (Evans et al., 1961). The interchange in position is inversely proportional to the square root of the molecular mass of this gas (Graham, 1833). This is described by Graham's law for n components and given by (Fahien, 1983; Farr, 1993; Evans et al., 1961)

$$\sum_{i=1}^{n} J_i \sqrt{M_i} = 0. \tag{16}$$

Therefore, the diffusion based on Graham's law, which includes

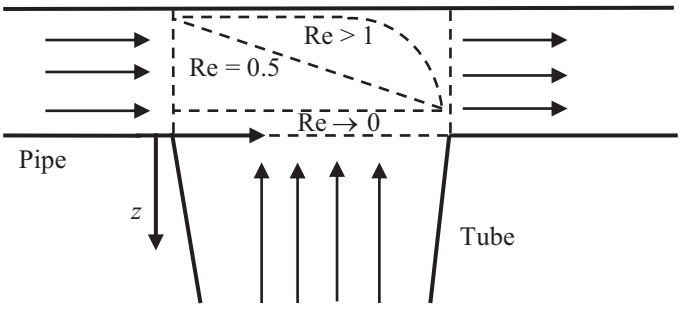

Fig. 3. Concentration profiles depending on the Reynolds number. High flowrates lead to a parabolic concentration profile ($Re > 1$) and an increased weighting of the influx concentration compared to the outflux one. The linear profile ($Re = 0.5$) yields the arithmetic mean of influx and outflux concentrations. For $Re \to 0$, the profile is horizontal meaning that the gases are ideally mixed.

the MSE (Eq. (11)) and a correction term, is given by (Farr, 1993)

$$J_i^{\text{Graham}} = J_i - x_i \frac{\sum_{i=1}^{n} \sqrt{M_i} J_i}{\sum_{i=1}^{n} \sqrt{M_i} x_i} \tag{17}$$

with M_i as the molar mass of species i. Eq. (17) is based on the concept of the Graham-average velocity which takes into account the drift effects caused by a superimposed viscous flow. For more mathematical details reference is made to Farr (1993). While this approach is mainly used for gaseous applications, the equimass countercurrent diffusive flux is mainly used for hydrologic applications (Farr, 1993) and proposed by Hassanizadeh and Gray (1979), Pollock (1986) and Falta et al. (1989', 1992). It ensures that the total diffusive mass flux summed over n components is zero (Evans et al., 1961)

$$\sum_{i=1}^{n} j_i = \sum_{i=1}^{n} J_i M_i = 0 \tag{18}$$

with j_i as the diffusive mass flux of species i and $j_i = J_i M_i$. The equimass diffusive flux is taken as the diffusive flux of the MSE, Eq. (11), including the correction term as well (Farr, 1993)

$$J_i^{\text{eqmass}} = J_i - x_i \frac{\sum_{i=1}^{n} M_i J_i}{\sum_{i=1}^{n} M_i x_i}, \tag{19}$$

where equilibrium values are used for x_i.

Eqs. (11), (17) and (19) require the knowledge of the concentration gradient. However, the correction terms of Eqs. (17) and (19) are assumed to be constant to allow for an analytical model, although the composition x_i in the tube changes.

Hence, the diffusive fluxes J_i can be replaced by using the MSE, inserting Eq. (11) into Eq. (15),

$$\frac{d}{dz}\left(\sum_{j=1}^{n-1} D_{ij}\frac{dx_j}{dz}\right) + \frac{1}{A_{\text{tube}}}\frac{dA_{\text{tube}}}{dz}\sum_{j=1}^{n-1} D_{ij}\frac{dx_j}{dz} = 0. \tag{20}$$

Now, assuming constant diffusivities to get an analytical model, although they change with the composition, and using Eq. (11), we obtain the steady-state Fick–Jacobs equation (Fick, 1855)

$$\frac{d^2 x_i}{dz^2} + \frac{1}{A_{\text{tube}}}\frac{dA_{\text{tube}}}{dz}\frac{dx_i}{dz} = 0. \tag{21}$$

The tube is assumed to be a cone with slightly varying radius $R_{\text{tube}}(z)$ and length L_{tube} and has the slight inclination $m = (R_{\text{tube}}^{(L)} - R_{\text{tube}}^{(0)})/L_{\text{tube}}$ with the boundary values $R_{\text{tube}}(z=0) = R_{\text{tube}}^{(0)}$ and $R_{\text{tube}}(z=L) = R_{\text{tube}}^{(L)}$. Thus, the tube cross section as a function of z and its derivation are

$$A_{\text{tube}}(z) = \pi\left(R_{\text{tube}}^{(0)} + mz\right)^2,\ \frac{dA_{\text{tube}}}{dz} = 2\pi m\left(R_{\text{tube}}^{(0)} + mz\right), \tag{22}$$

and we obtain the following expression:

$$\frac{1}{A_{\text{tube}}}\frac{dA_{\text{tube}}}{dz} = \frac{2m}{R_{\text{tube}}^{(0)} + mz}. \tag{23}$$

Inserting Eq. (23) into Eq. (21), the solution of the Fick-Jacobs equation is

$$x_i(z) = x_i^{(0)} + \left(x_i^{(L)} - x_i^{(0)}\right)\left(\frac{z}{L_{\text{tube}}\Lambda + (1-\Lambda)z}\right) \tag{24}$$

with Λ being the ratio of $R_{\text{tube}}^{(0)}$ to $R_{\text{tube}}^{(L)}$, leading to $\Lambda = 1$ for a uniform tube and the boundary conditions

$$x_i(z=0) = x_i^{(0)},\ x_i(z=L) = x_i^{(L)}. \tag{25}$$

Differentiation of Eq. (24) leads to

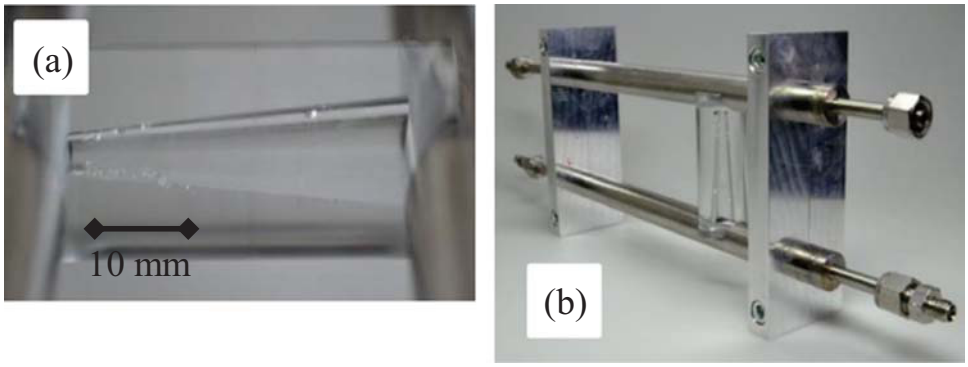

Fig. 4. Conical test tube made of PMMA with ratio of tube radii $\Lambda = 2.7$. (a) The conical shape is obtained by the use of a tapered reamer. (b) The ends of the tube are connected to the pipes made of stainless steel. A press fit is created on each end of the tube to center it against the bore holes in the pipes and to stabilize the connection.

$$\frac{dx_i}{dz} = \frac{\Lambda L_{\text{tube}}}{\left(\Lambda L_{\text{tube}} - \Lambda z + z\right)^2}\left(x_i^{(L)} - x_i^{(0)}\right) \tag{26}$$

and to obtain the gradient in Eq. (11), we write

$$\left.\frac{dx_i}{dz}\right|_{z=0} = \frac{1}{\Lambda}\frac{x_i^{(L)} - x_i^{(0)}}{L_{\text{tube}}}. \tag{27}$$

Inserting Eqs. (11) and (27) into Eq. (8) leads to

$$n_i^{(0,y_0)} = n_i^{(0,0)} - \frac{A_{\text{tube}}^{(0)}}{A_{\text{pipe}}}\left(-\frac{c_t}{\Lambda L_{\text{tube}}}\sum_{j=1}^{n-1} D_{ij}\left(x_j^{(L)} - x_j^{(0)}\right)\right). \tag{28}$$

With the derivation of Eq. (28), we insert an analytical solution for the diffusive flux in the tube into the component mass balance. The required gradient is represented by the boundary conditions of the tube whereby its geometry is considered by Λ.

The expression according to Eq. (28) already indicates that the diffusion rate through a cone with identical average cross section (see Fig. 2a) is lower by the factor of $A_{\text{tube}}^{(0)}/\Lambda$ compared to the uniform tube. This is due to fact that the linear concentration profile for the uniform tube, is the shortest possible profile (Fig. 2b). Hence, the integral of the local driving force gets lower with increasing Λ. With other words, the larger the disparity of $A_{\text{tube}}^{(0)}$ and $A_{\text{tube}}^{(L)}$ the longer the curve of the concentration profile and the lower the diffusion rate.

2.4. Model solution and analysis

When considering the convective influx with a constant volumetric flowrate $\dot{F}_{\text{pipe}}^{(0,0)}$ in pipe A given by

$$n_i^{(0,0)} = c_t x_i^{(0,0)} \frac{\dot{F}_{\text{pipe}}^{(0,0)}}{A_{\text{pipe}}}, \tag{29}$$

the convective outflux at $y_0 = d^{(0)}$ can be calculated as

$$n_i^{(0,d^{(0)})} = c_t x_i^{(0,0)} \frac{\dot{F}_{\text{pipe}}^{(0,0)}}{A_{\text{pipe}}} - \frac{A_{\text{tube}}^{(0)}}{A_{\text{pipe}}}\left(-\frac{c_t}{\Lambda L_{\text{tube}}}\sum_{j=1}^{n-1} D_{ij}\left(x_j^{(L)} - x_j^{(0)}\right)\right) \tag{30}$$

with known molar fractions $x_i^{(0,0)}$ of each species i at the inlet. Then, the molar fraction of each species i of the outflux, $x_i^{(0,d^{(0)})}$, can be determined correspondingly to Eq. (29) as

$$x_i^{(0,d^{(0)})} = x_i^{(0,0)} - \frac{A_{\text{tube}}^{(0)}}{\dot{F}_{\text{pipe}}^{(0,0)}}\left(-\frac{1}{\Lambda L_{\text{tube}}}\sum_{j=1}^{n-1} D_{ij}\left(x_j^{(L)} - x_j^{(0)}\right)\right). \tag{31}$$

To get a solution based on Graham's law, the bracketed diffusion term in Eq. (31) is replaced by the adapted Eq. (17). Hence we obtain

Table 1
Dimensions of pipes and test tubes.

Element	Symbol	Dimension
Cross section pipes A, B	A_{pipe}	132.73 mm^2
Radius pipes A, B	R_{pipe}	6.5 mm
Uniform tube		
Length	L_{tube}	95 mm
Cross section	A_{tube}	28.27 mm^2
Radius	R_{tube}	3 mm
Conical tube		
Length	L_{tube}	51 mm
Large cross section	$A_{\text{tube}}^{(0)}$	51.53 mm^2
Small cross section	$A_{\text{tube}}^{(L)}$	7.07 mm^2
Average cross section	$\bar{A}_{\text{tube}}$	29.30 mm^2
Large radius	$R_{\text{tube}}^{(0)}$	4.05 mm
Small radius	$R_{\text{tube}}^{(L)}$	1.50 mm
Radius ratio	$\Lambda = R_{\text{tube}}^{(0)}/R_{\text{tube}}^{(L)}$	2.7

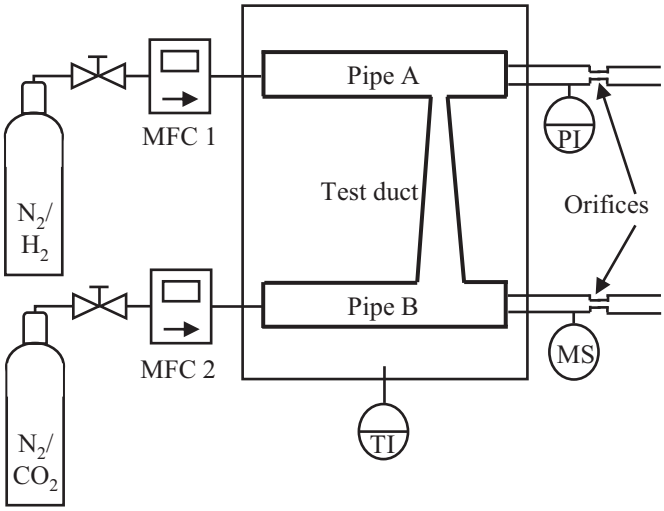

Fig. 5. Experimental setup used for the diffusion experiments. Different test tubes are implemented between pipes A and B, contained in an isolated box. The temperature in the box is measured with a resistance thermometer. The absolute pressure of the outflux is measured with a pressure sensor integrated in the one pipe while the molar fraction is analyzed online using a mass spectrometer integrated in the other pipe. Pressure sensor and mass spectrometer are adapted with SWAGELOK connections and can be changed easily.

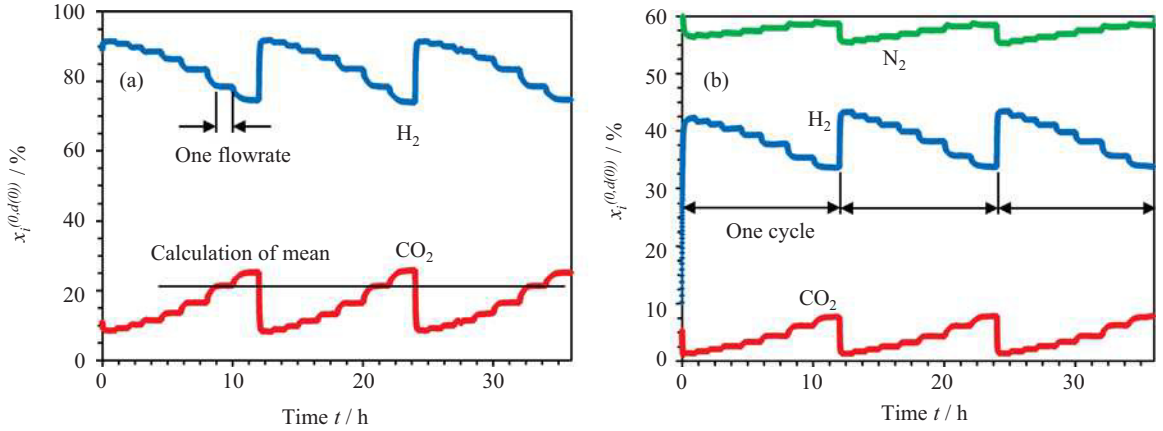

Fig. 6. Recording of the outflux molar fractions, experiment of the binary (a) and ternary system (b). Each step in the graphs stands for one flowrate and eight steps correspond a cycle. The exemplary horizontal line in (a) indicates the calculation of the mean molar fraction for a given mass flowrate during each cycle.

$$x_i^{\left(0,d^{(0)}\right)}=x_i^{(0,0)}-\frac{A_{\text{tube}}^{(0)}}{\dot{F}_{\text{pipe}}^{(0,0)}} \cdot\left(-\frac{\sum_{j=1}^{n-1}D_{ij}\left(x_j^{(L)}-x_j^{(0)}\right)}{\Lambda L_{\text{tube}}}-x_i\frac{\sum_{i=1}^{n}\sqrt{M_i}\left(-\frac{1}{\Lambda L_{\text{tube}}}\sum_{j=1}^{n-1}D_{ij}\left(x_j^{(L)}-x_j^{(0)}\right)\right)}{\sum_{i=1}^{n}\sqrt{M_i}x_i}\right) \quad (32)$$

and correspondingly for equimass diffusion with adapted Eq. (19)

$$x_i^{\left(0,d^{(0)}\right)}=x_i^{(0,0)}-\frac{A_{\text{tube}}^{(0)}}{\dot{F}_{\text{pipe}}^{(0,0)}} \cdot\left(-\frac{\sum_{j=1}^{n-1}D_{ij}\left(x_j^{(L)}-x_j^{(0)}\right)}{\Lambda L_{\text{tube}}}-x_i\frac{\sum_{i=1}^{n}M_i\left(-\frac{1}{\Lambda L_{\text{tube}}}\sum_{j=1}^{n-1}D_{ij}\left(x_j^{(L)}-x_j^{(0)}\right)\right)}{\sum_{i=1}^{n}M_ix_i}\right). \quad (33)$$

Based on the results of Veltzke et al. (2015) for instationary multicomponent diffusion, it is assumed for the upper system of mix 1 in Fig. 1b that hydrogen leaves the system at z=0 while nitrogen as well as carbon dioxide enter the system at the very same position. In order to calculate the molar fractions of each outflux species i, we assume the initial boundary molar fractions of the duct to be the same as the known molar fractions of the influxes, as in Ref. Fahien (1983), with

$$x_i^{\text{initial}}(z=0)=x_i^{(0)}=x_i^{(0,0)},\ x_i^{\text{initial}}(z=L)=x_i^{(L)}=x_i^{(L,0)}. \quad (34)$$

We have to take into account that the gas velocity in the pipes in the experiment is greater than zero. Therefore we have to note that the gas velocity in the pipes influences the iterative approximation of outflux gas concentrations. The dimensionless Reynolds number (see Eq. (3)) is estimated to consider this effect and to be applied as a weighting factor during iteration.

Therefore, the boundary molar fractions are taken as the weighted mean of the influx and outflux molar fractions

$$x_i(z=0)=x_i^{(0)}=Re^{(0,0)}x_i^{(0,0)}+\left(1-Re^{(0,0)}\right)x_i^{\left(0,d^{(0)}\right)},$$
$$x_i(z=L)=x_i^{(L)}=Re^{(L,0)}x_i^{(L,0)}+(1-Re^{(L,0)})x_i^{(L,d^{(L)})}. \quad (35)$$

Here, exemplary concentration profiles in the pipe subject to different Reynolds numbers Re are depicted in Fig. 3.

As depicted in Fig. 3, high gas flowrates with $Re>1$ cause a parabolic concentration profile and a reinforced weighting of the influx concentration. Hence, the high gas velocity leads to an increased weighting of the influx concentration, $k^{(0)}\gg(1-k^{(0)})$. Furthermore, a linear profile represents the arithmetic mean value of influx and outflux concentrations, $k^{(0)}\gg(1-k^{(0)})=0.5$. Finally, a horizontal, constant concentration profile stands for an ideally mixed gas and is caused by very low gas velocities and an increased weighting of the outflux concentration, $k^{(0)}\ll(1-k^{(0)})$.

Regarding Eq. (32), we expect that diffusion is delayed in conical tubes and that the flowrate $\dot{F}$ to reach a certain concentration is maximum for the uniform one. For this reason, we equate Eq. (32) in the case of a cone and in the case of a uniform tube with diffusion based on Graham's law. We obtain

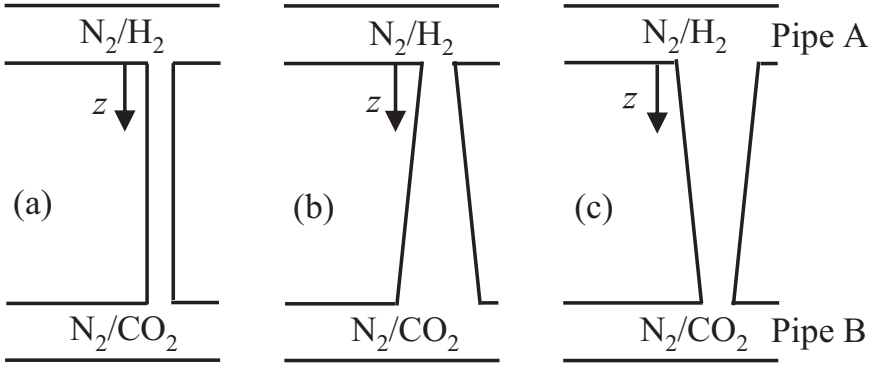

Fig. 7. Different settings for the test tubes, (a) uniform tube, conical tube in (b) diverging and (c) converging direction along z-coordinate.

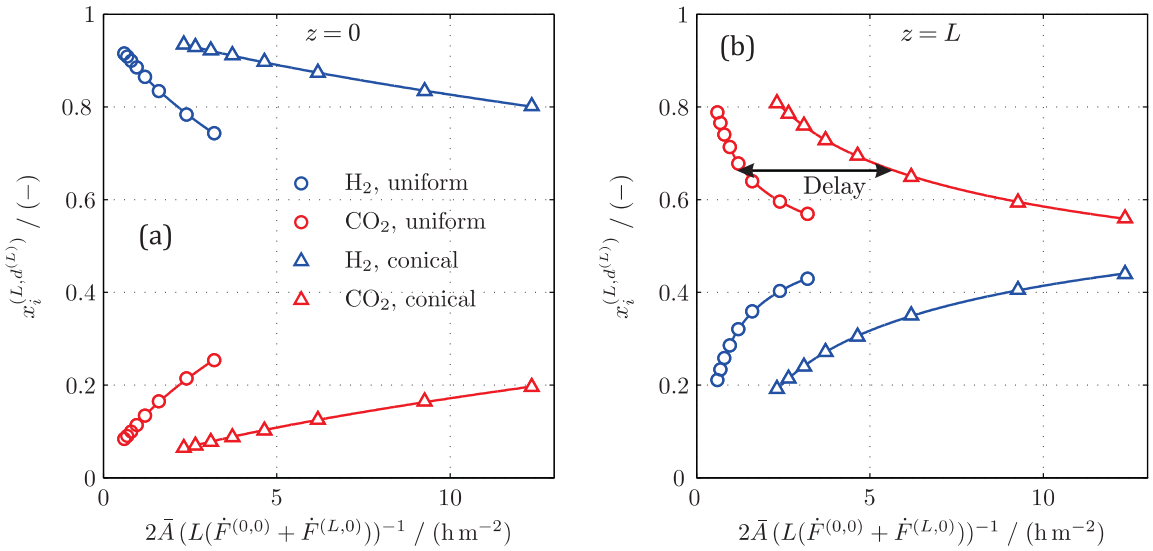

Fig. 8. Measured molar fractions for the binary diffusion experiments in pipe A (a) and pipe B (b). All experiments are carried out at $p \approx 1$ bar and $T \approx 25$ °C. The curves are fitted to the data using a power-law function for further analysis.

$$\frac{A^{(0)}_{\text{tube,cone}}}{\Lambda L_{\text{tube,cone}} F^{(0,0)}_{\text{pipe,cone}}}\left(\sum_{j=1}^{n-1} D_{ij}\left(x_j^{(L)} - x_j^{(0)}\right) - x_i \frac{\sum_{i=1}^{n}\sqrt{M_i}\sum_{j=1}^{n-1} D_{ij}\left(x_j^{(L)} - x_j^{(0)}\right)}{\sum_{i=1}^{n}\sqrt{M_i}x_i}\right)$$
$$= \frac{A_{\text{tube,uni}}}{L_{\text{tube,uni}} F^{(0,0)}_{\text{pipe,uni}}}\left(\sum_{j=1}^{n-1} D_{ij}\left(x_j^{(L)} - x_j^{(0)}\right) - x_i \frac{\sum_{i=1}^{n}\sqrt{M_i}\sum_{j=1}^{n-1} D_{ij}\left(x_j^{(L)} - x_j^{(0)}\right)}{\sum_{i=1}^{n}\sqrt{M_i}x_i}\right) \quad (36)$$

and shortening yields

$$\alpha^* = \frac{\dot{F}^{(0,0)}_{\text{pipe,uni}}}{\dot{F}^{(0,0)}_{\text{pipe,cone}}} = \Lambda \frac{L_{\text{tube,cone}}\, A_{\text{tube,uni}}}{L_{\text{tube,uni}}\, A^{(0)}_{\text{tube,cone}}} \quad (37)$$

with defining the hindrance factor α^*. Regarding Eq. (37), α^* of the stationary diffusion process agrees with that one of the instationary diffusion process in Veltzke et al. (2015) and is independent of the assumed diffusion process, either Graham's law or equimass diffusion. Assuming that the uniform and conical tubes have an identical length and average cross section $A_{\text{tube,uni}} = \bar{A}_{\text{tube,cone}} = \pi/2\,(R^{(0)2} + R^{(L)2})$, the hindrance factor is

$$\alpha^* = \frac{R^{(0)2} + R^{(L)2}}{2R^{(0)}R^{(L)}} > 1 \text{ for } A_{\text{tube,uni}} = \bar{A}_{\text{tube,cone}}; L_{\text{tube,uni}} = L_{\text{tube,cone}}. \quad (38)$$

The hindrance factor $\alpha^* > 1$ indicates that diffusion is delayed in conical tubes, since we obtain the highest flowrate to get a certain outflux molar fraction with the uniform tube. For each conical tube, the flowrate has to be lower for the gases to reach the same outflux molar fractions. Furthermore, α^*only depends on the disparity of $R^{(0)}$ and $R^{(L)}$ and it is indifferent whether $R^{(0)}$ or $R^{(L)}$ is larger, hence the direction of the cone (converging or diverging) does not affect the hindrance effect.

2.5. Properties of gases and gas mixtures

The predictive calculation of all molar fractions in the outfluxes requires the calculation of the binary diffusivities $\mathcal{D}_{ij}$ for species i and j. As mentioned previously, the binary diffusivities can be estimated by using the Chapman-Enskog kinetic theory. In this work, a temperature of 298.15 K and a pressure of 1 atm in the system are used for the calculations, hence, we obtain $\mathcal{D}_{H_2/N_2} = 7.5884{\cdot}10^{-5}$ m^2 s^{-1}, $\mathcal{D}_{H_2/CO_2} = 6.3221{\cdot}10^{-5}$ m^2 s^{-1} and $\mathcal{D}_{N_2/CO_2} = 1.5047{\cdot}10^{-5}$ m^2 s^{-1} (Bird et al., 2007).

The calculation of the Reynolds numbers of both influxes requires the densities and the viscosities of the influx gases at 298.15 K and 1 atm. With respect to the binary system, we took the density of hydrogen as $\rho_{H_2} = 0.0824$ kg m^{-3} and that of carbon

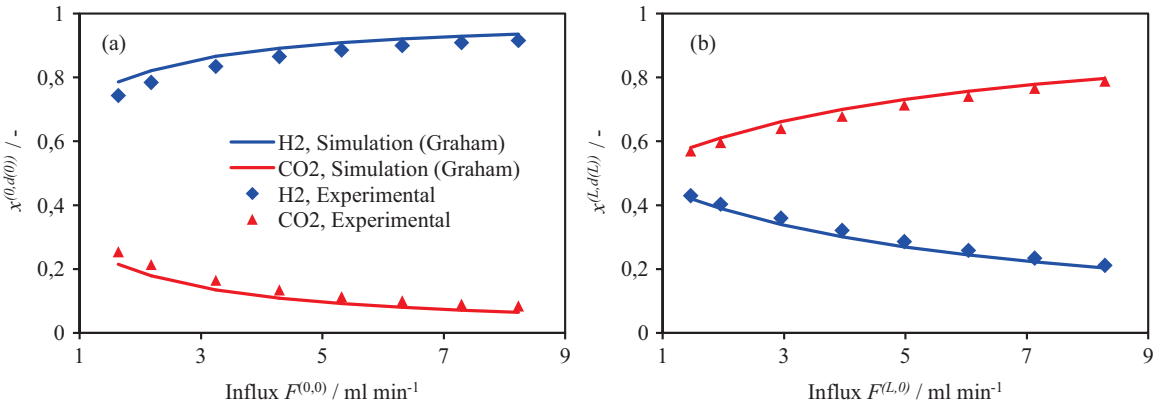

Fig. 9. Comparison of calculations using the analytical model according to Eq. (32) and experimental results for binary diffusion in the *uniform* tube.

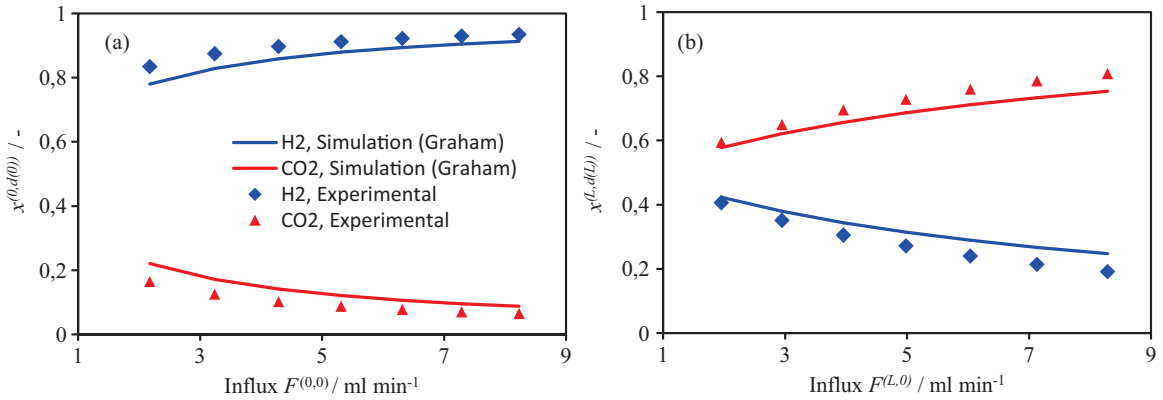

Fig. 10. Comparison of calculations using the analytical model according to Eq. (32) and experimental results for binary diffusion in the *conical* tube.

dioxide as $\rho_{CO_2} = 1.808$ kg m^{-3}. For the ternary system, the mixture density of H_2/N_2 is $\rho_{H_2/N_2} = 0.6136$ kg m^{-3} and that one of N_2/CO_2 is $\rho_{N_2/CO_2} = 1.4750$ kg m^{-3}. The viscosities are $\eta_{H_2} = 8.925 \cdot 10^{-6}$ Pa s and $\eta_{CO_2} = 14.73 \cdot 10^{-6}$ Pa s and $\eta_{H_2/N_2} = 16.26 \cdot 10^{-6}$ Pa s and $\eta_{N_2/CO_2} = 16.55 \cdot 10^{-6}$ Pa s, respectively. Furthermore, the molar mass of hydrogen is $M_{H_2} = 2.016$ g mol^{-1}, that one of nitrogen is $M_{N_2} = 28.01$ g mol^{-1} and that one of carbon dioxide is $M_{CO_2} = 44.01$ g mol^{-1}. The molar masses of the mixtures are obtained as the arithmetic mean (Bronskhorst High-Tech).

3. Experimental

This part deals with the manufacturing process of the used test tubes, followed by the description of the experimental setup. Also, the experimental procedure is described in detail.

It is to note that the experimental challenge of this work was to ensure that convection within the test tubes does not occur since we want to study *pure* diffusion. The different gases and gas mixtures perfusing the pipes, however, possess varying characteristics which may lead to different pressure drops and thus to a pressure gradient in the tube. Hence, the correct flow rate ratio for both pipes has to be determined to avoid a pressure difference and the resulting convection within the tube. In this context we developed an experimental procedure to estimate the correct ratio which is provided in Appendix B.

3.1. Test tubes

The steady-state diffusion experiments are performed with two different test tubes. The first one applied is a uniform tube, made of stainless steel with an inner diameter of 6 mm. Further, a conical tube is made of polymethylmethacrylate (PMMA) that has a linearly changing radius. This cone is produced by the application of a tapered reamer and the result is depicted in Fig. 4a. All dimensions of the test tubes are provided in Table 1.

3.2. Experimental setup

According to Fig. 4b, the test tubes are assembled between two identical pipes (13 mm inner diameter, made of stainless steel). The uniform tube is soldered on each pipe, but the conical tube is connected to the pipes by a press fit, sealed with glue. The construction of the connection between a tube and the pipes shown in Fig. 4b also works as a centering and stabilization device.

The device according to Fig. 4 is assembled into the experimental setup depicted in Fig. 5. Each of two gas reservoirs (either pure H_2 and CO_2 or N_2/H_2 gas mixture with $x_{H_2} = 0.5012$,

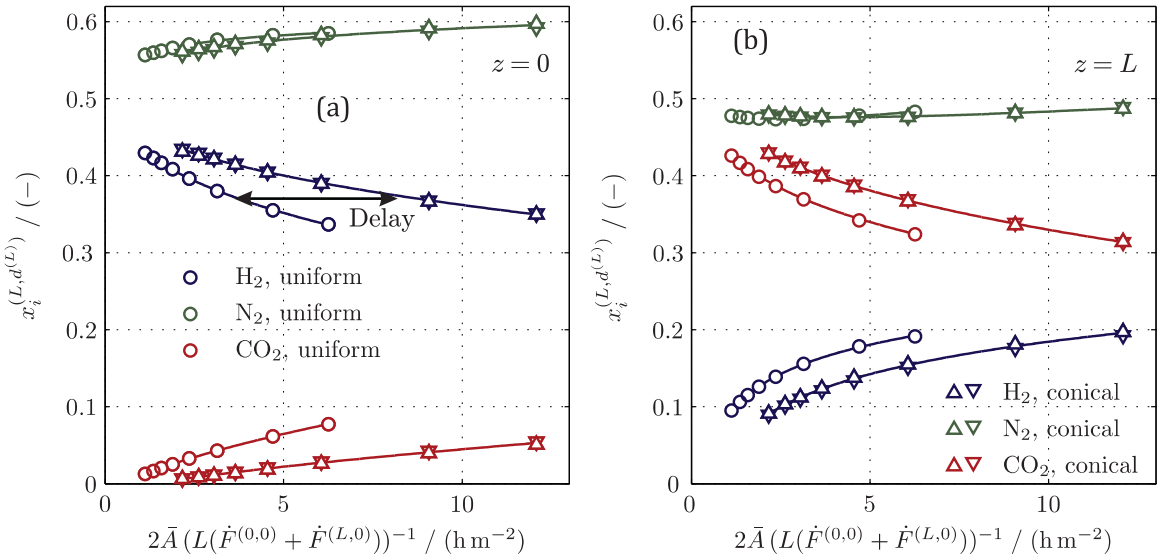

Fig. 11. Measured molar fractions for the ternary diffusion experiments in pipe A (a) and pipe B (b). All experiments are carried out at $p \approx 1$ bar and $T \approx 25$ °C. The curves are fitted to the data using a power-law function for further analysis.

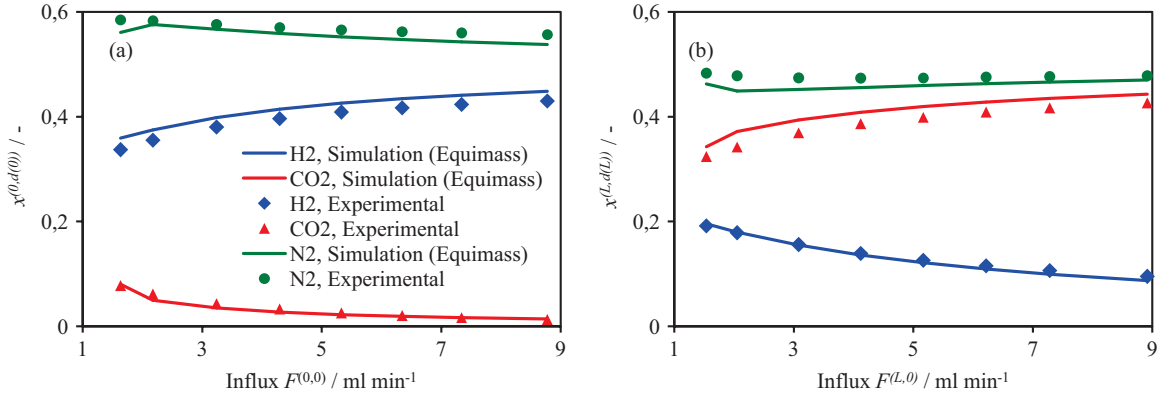

Fig. 12. Comparison of calculations using the analytical model according to Eq. (33) and experimental results for ternary diffusion in the *uniform* tube.

$x_{N_2}=0.4978$ and N_2/CO_2 gas mixture with $x_{N_2}=0.5016$, $x_{CO_2}=0.4963$ (Veltzke et al., 2015), Linde AG) is connected to one of the two pipes and the gas mixture flowrates are controlled by mass flow controllers, MFC 1 and MFC 2 (both F 201CV-ABD-11-Z, Bronkhorst).

According to Fig. 5, an orifice and a long hose after each pipe prevent back diffusion of ambient air into the pipes.

Temperature variations in the pipes and the test tube are damped by a box filled with isolation material and the temperature in the box is measured by a Pt 1000 resistance thermometer (TF35, Wika SE & Co. KG, Germany). A pressure sensor (PMP 5076, GE, USA) is connected subsequent to one of the pipes and a mass spectrometer (GAM200, InProcessInstruments GmbH, Germany) subsequent to the other one, which is used to measure the species composition of the outflux in one pipe permanently. Pressure sensor and mass spectrometer are connected with SWAGELOK adapters and can be changed easily.

3.3. Experimental procedure

During the diffusion experiments, the standard mass flow rate of MFC 1 is decreased from 8.5 ml N min^{-1} to 1.5 ml N min^{-1} in consideration of the required waiting times until steady state is reached. In preliminary tests we observed that steady state conditions of the species composition is reached after 60 min for a mass flowrate under standard conditions (0 °C, 1 atm) $\acute{M} \geq 6$ ml N min^{-1}, after 90 min for 6 ml N min$^{-1} > \acute{M} \geq 4$ ml N min^{-1} and after 120 min for $\acute{M} < 4$ ml N min^{-1}. Hence, a cycle with eight different flowrates requires approximately 12 h (Fig. 6).

For each experiment, always three cycles, each with eight different flowrates, are recorded and the outflux molar fractions are plotted against the time. Each step in the graphs in figure corresponds to one flowrate. In this figure, (a) exemplarily shows an experiment with the binary system (H_2/CO_2) while (b) shows an experiment with the ternary system ($H_2/N_2/CO_2$).

Finally, the arithmetic mean of the molar fraction is calculated for each step which results in eight data points for each experimental setting.

We want to emphasize that during a second run, the positions of pressure sensor and mass spectrometer are exchanged while the flow conditions remained identical. This allows us to obtain the molar fractions in both pipes.

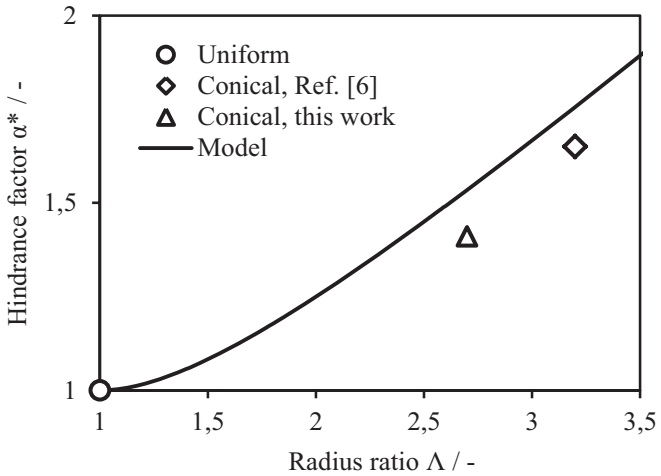

Fig. 14. Theoretical hindrance factor and experimentally observed delay as a function of the radius ratio. The experimental data point of the current work (upright triangle) is obtained by using Eq. (40) on basis of all, binary and ternary, experiments (as arithmetic mean). The errorbar is smaller than the symbol.

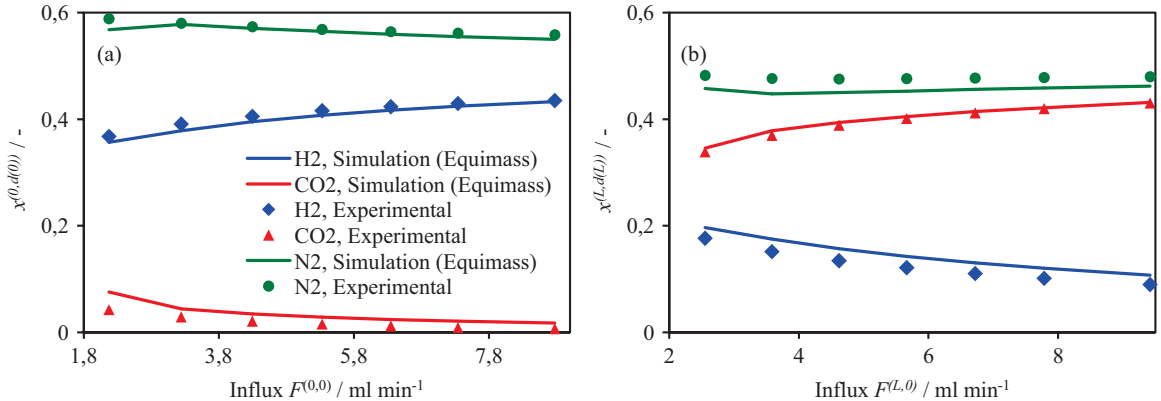

Fig. 13. Comparison of calculations using the analytical model according to Eq. (33) and experimental results for ternary diffusion in the *conical* tube.

After doing the experiments with the uniform tube (Fig. 7a), the conical tube is assembled twofold between pipes A and B: in diverging (Fig. 7b) and converging direction (Fig. 7c) along the z-coordinate.

All experiments are carried out for the case of the binary mixture (H_2/CO_2) and the case of the ternary mixture ($H_2/N_2/CO_2$). Pressure and temperature always were almost identical ($p \approx 1$ bar; $T \approx 25$ °C) with slight variations subject to changings of ambient conditions.

As figured out earlier, one of the basic assumptions of this work is the isobaric condition between the pipes (infinite gas reservoirs) meaning the absence of a pressure gradient from the one end of the test tube to the other. Therefore, an experimental determination of the optimal mass flow rate ratio of both streams was carried out. This is explained in detail in Appendix B.

4. Results and discussion

In this section, we present the experimental as well as the simulation results of both the binary and the ternary system. The experimental procedure in Section 3.3 is applied to the binary system with the influx of H_2 at $z=0$ and that one of CO_2 at $z=L_{duct}$ in the following section and to the ternary system with the influx of H_2/N_2 at $z=0$ and that one of N_2/CO_2 at $z = L_{tube}$ in Section 4.2.

4.1. Binary counter diffusion

The molar fractions of both species measured with the mass spectrometer in pipe A ($z = 0$) are plotted versus the inversed sum of the influx volumetric flowrates (Fig. 8a). In order to make different conical and uniform tubes comparable, we scaled this value with the dimensions of the test tubes (length and mean cross section) provided in Table 1. Hence, the value of the abscissa has the dimension of time devided by m^2. The circles indicate the results obtained on the uniform tube while the triangles represent the results of the conical tube. The data points are fitted with a power-law function of the form $y = ax^b+c$ for further analysis. On the right-hand side, in Fig. 8b, the molar fractions measured in pipe B ($z = L_{tube}$) are depicted in the same way.

In general it can be observed that the concentration of H_2 in pipe A decreases with increasing abscissa value while the hydrogen concentration in pipe B increases. This means that with increasing flow velocity in the pipes the concentration of hydrogen in the carbon dioxide stream is decreased. This is reasonable since more pure carbon dioxide dilutes the mixture in the pipe and hence reduces the hydrogen concentration. The same but inverse effect applies for carbon dioxide. In all cases the molar fractions tend to converge to 0.5 which approximately is the average molar fraction of the volumetric influxes. The shape of the curves strikingly remind to the results of the instationary two-bulb-diffusion-experiment (Veltzke et al., 2015; Duncan and Toor, 1962) where the abscissa value has the identical unit. Hence, the inversed sum of the influx volumetric flowrates of the current stationary diffusion experiment can be interpreted as the duration of the instationary two-bulb-diffusion-experiment.

Most interesting although is the comparison between the uniform and the conical tube. The counter-diffusion of H_2 and CO_2 is significantly delayed by the conicity of the concial tube. This means that the diffusive transport in the conical tube is slower than in the uniform one. This finding qualitatively confirms the analysis of our model in Section 2.4. In order to obtain a quantitative measure of this delay effect, we define the delay as the horizontal distance between the fitted curves. In Section 4.3 we will provide further analysis on the theoretically developed hindrance factor α^* (Eq. (37)) and the experimentally observed delay.

Furthermore, the model developed in Section 2 is used for predictive calculations of the molar fractions for different influx volumetric flowrates. In Fig. 9 the experimental values for the uniform tube are compared to those calculated with Eq. (32) (using Graham's law).

In case of the calculations for the molar fractions in pipe A (tube position $z=0$, Fig. 9a) the calculated hydrogen concentrations are in quite good agreement to those obtained from the experiment. The deviation increases with decreasing volumetric influx. At the minimum volumetric flow rate the maximum deviation is approximately 5 % which indicates very good agreement between theory and experiment. The molar fractions calculated for CO_2 at the $z=0$ position are significantly lower than those of the experiment. Here the deviation decreases with the influx volumetric flow rate and the maximum deviation is approximately 30 % (see Table C1 in Appendix C).

Considering pipe B (tube position $z= L_{tube}$, Fig. 9b) we notice that calculations and experiment are in very good agreement for both species. The maximum deviation in case of hydrogen is 6.7 % while the deviation for the carbon dioxide data is always lower than 3.2 %. Here no dependency of deviation and influx volumetric flow rate can be observed (see Table C1 in Appendix C).

The observations for the comparison of model and experiment on the conical tube are slightly different. At the tube position $z=0$ (Fig. 10a) the deviation for hydrogen increases with decreasing volumetric flow rate which is the same behavior as for the uniform tube. No such dependency, however, can be observed for carbon dioxide, where the calculated values are significantly lower (which is converse to the discrepancy in the uniform tube).

At the tube position $z= L_{tube}$ (Fig. 10b) the deviation of the hydrogen values decreases with influx volumetric flow rate and the deviation is significantly higher than observed for the uniform tube. The values calculated for carbon dioxide, however, are in quite good agreement to the experimental ones. All results for the case of binary diffusion in the conical tube are additionally provided in Table C2 in Appendix C.

4.2. Ternary co- and counter-diffusion

Fig. 11 shows the results of the ternary mixture experiments. Again, on the left-hand side (Fig. 11a) the molar fractions measured in pipe A are plotted versus the abscissa values as defined in Section 4.1. The right-hand side (Fig. 11b) shows the measurements in pipe B at tube position $z= L_{tube}$.

In both plots the molar fractions of hydrogen and carbon dioxide tend to converge to 0.25 which approximately is the average concentration of the volumetric influxes. The curves show the same behavior as for the binary diffusion experiments shown in Fig. 8. The nitrogen concentration in pipe A increases with the abscissa value while it slightly increases in pipe B. This effect is due to co-diffusion (Duncan and Toor, 1962; Taylor and Krishna, 1993; Evans et al., 1961) meaning that nitrogen molecules are dragged by the diffusing carbon dioxide towards the hydrogen stream. Logically, this effect increases with decreasing flow velocity in the pipes (see Section 4.1).

Focusing now on the comparison between the uniform tube and the conical one we can observe the same delay effect as for the binary diffusion. The co-diffusion of nitrogen as well as the counter-diffusion of carbon dioxide and hydrogen is significantly slower in the conical tube. From this we can conclude that the diffusion delay does not depend on composition. Also we can show that direction of the cone (diverging/converging, see Fig. 7) does not have any effect on the results as it was theoretically found in Section 2.4.

Again, the model developed in Section 2 is used for predictive calculations of the molar fractions for different influx volumetric

flowrates. In Fig. 12 the experimental values for the uniform tube are compared to those calculated with Eq. (33) (using equimass diffusion).

For the uniform tube the agreement between model and experiment is strikingly good. The deviation is mostly at the order of magnitude of 5 %. Only for very low absolute molar fractions (for instance carbon dioxide in pipe A) the deviation increases to 20 %. All results for the case of ternary diffusion in the uniform tube are provided in Table C3 in Appendix C.

The same occurs for the conical tube with the results shown in Fig. 13. While the model matches the experiment extremely good for medium molar fractions, significant deviations are observed for very low absolute concentrations. However, if we correlate the deviation with the absolute value of the molar fraction, we obtain the relative deviation as being always lower than 7%. Again, all results for the case of ternary diffusion in the conical tube are provided in Table C4 in Appendix C.

One possible explanation for the partly significant discrepancies is the simplifying assumption according to Eq. (6). In reality, the changing of the species concentration does change the diffusion rate which again changes the convection in the pipe due to the dependency of the convective flow rate on, e.g., density and viscosity. This might explain why high discrepancies occur systematically for particular "combinations" of gas species and pipes while for other species/pipes the discrepancy is negligible.

Nevertheless, we can conclude that the developed model subject to equimass diffusion describes the experimental results for the ternary diffusion very good.

4.3. Diffusion delay

As mentioned in Section 4.1 we used the parameters of the fitted power-law function for a quantitative analysis of the delay effect which is the distance between the curve of the uniform tube and that one of the conical one. For subtraction of both curves we inverted the power-law function to

$$\left(\frac{y_j - c_j}{a_j}\right)^{-b_j} = x_j \text{ with } j\text{=uniform, cone} \tag{39}$$

where x is the abscissa value $2\bar{A}\,(L\,(\dot{F}^{(0,0)} + \dot{F}^{(L,0)}))^{-1}$ and y is the ordinate value x_i. By that we define the experimental hindrance factor as

$$\alpha^{*}_{\text{exp}} = 1 + \left|\frac{x_{\text{uniform}} - x_{\text{cone}}}{x_{\text{uniform}} + x_{\text{cone}}}\right| \tag{40}$$

which is the relative offset of both curves. According to Eq. (40) we calculated α^{*}_{exp} for all four curve pairs of the binary case and all the six curve pairs of the ternary case. Those ten values are averaged and the standard deviation is calculated. We obtained $\alpha^{*}_{\text{exp}} = 1.3962 \pm 0.0119$ meaning that the diffusion in the conical tube is delayed by approximately 40 % compared to the uniform one.

In Fig. 14 this experimentally derived hindrance factor is compared to the hindrance factor predicatively calculated according to Eq. (38). The calculations show, that the hindrance factor increases with the ratio of inlet radius to outlet radius Λ. This means, that the delay related to the uniform case increases with conicity of the tube. Furthermore, the hindrance factor experimentally obtained for a conical tube with $\Lambda = 3.16$ in Veltzke et al. (2015) is shown here. As can be seen by this plot, the theoretical prediction and the experimental results on two test tubes used in two totally different experimental setups are in good agreement.

Consequently, the diffusive flux in a tapered tube is always lower compared to that one in a uniform one with identical average cross section A_{tube}. Furthermore, this effect increases with Λ whereby it is indifferent whether $R^{(L)}_{\text{tube}}$ or $R^{(0)}_{\text{tube}}$ is larger.

5. Conclusion

Steady-state binary and multicomponent gas diffusion is studied in tubes of different geometries, namely uniform and conical. For this purpose, a novel diffusion experiment is developed and described theoretically by a mathematical model. Compared to the transient two-bulb-diffusion-experiment, the presented stationary approach allows for much faster measurements. The results, however, are transferable since the volumetric flow rate in the stationary case is inversely proportional to the experimental duration in the transient case.

A comparison of diffusing gases in different tube geometries shows a delayed diffusion process for conical tubes compared to uniform ones with constant cross section, independent of the orientation of the tube (converging or diverging). Delayed diffusion is proven during the experiments and the simulation results. By means of model calculations, we confirm that the hindrance increases with the ratio of inlet and outlet radius, Λ. Due to the low rarefaction of the gas this effect cannot be associated to gas interactions with the wall but rather to changes in local volumes along the longitudinal axis. In fact it was shown that the phenomenon of delayed diffusion can be explained by means of the integral of the local driving force which reduces with increasing Λ. Additionally, it is worth noting that delayed steady-state diffusion under non-rarefied conditions is independent of the diffusion mechanism, either Fickian diffusion in the binary system or multicomponent Maxwell–Stefan diffusion in the ternary system. In fact this delay effect is rather caused by volumetric changes in longitudinal direction of the tapered pore.

Consequently, for gaseous diffusion in “real” pores, that typically are somehow tapered, the transport limitation is even more serious than considered so far.

Acknowledgment

This work was financially supported by the German Research Foundation (DFG) through funding VE 808/1-1. We want to thank Lars Kiewidt for the interesting and fruitful discussions.

Appendix A

Symbol	Description	Unit
A_{pipe}	Pipe cross section	m^2
$\bar{A}_{\text{tube,cone}}$	Average cross section of cone	m^2
$A^{(0)}_{\text{tube}}$, $A^{(L)}_{\text{tube}}$	Tube cross at $z=0$ and $z=L$	m^2

α^*, α^*_{exp}	Theoretical and experimental hindrance factor	dimensionles
c_t	Total molar concentration	mol m^{-3}
$d^{(0)}_{tube}$, $d^{(L)}_{tube}$	Tube diameter at $z=0$ and $z=L$	m
$Đ_{ij}$	Binary diffusivity of species i in j	m^2 s^{-1}
$Đ_{ij}$	Maxwell-Stefan binary diffusivities	m^2 s^{-1}
D_{ij}	Multicomponent diffusivity	m^2 s^{-1}
$\dot{F}^{(0,0)}_{pipe}$	Influx volumetric flowrate in the pipe	m s^{-1}
j_i	Diffusive mass flux	kg s^{-1}
$J^{eqmol,(0)}_i$	Equimolar diffusion rate	mol s^{-1}
J^{Graham}_i	Graham diffusion rate	mol s^{-1}
$J^{(0)}_i$, $J^{(L)}_i$	Diffusion rate at $z=0$ and $z=L$	mol s^{-1}
L_{tube}	Tube length	m
λ	Mean free path	m
$\Lambda = R^{(0)}_{tube}/R^{(L)}_{tube}$	Ratio of tube radii	dimensionless
m	Inclination	a.u.
M	Molar mass	g mol^{-1}
$\acute{M}$	Mass flowrate under standard conditions	ml N min^{-1}
$\acute{M}^*$	Mass flow rate ratio	dimensionless
η	Dynamic viscosity	Pa s
$N^{(0)}_i$, $N^{(L)}_i$	Amount of species at $z=0$ and $z=L$	mol
$n_i^{(0,d^{(0)})}$, $n_i^{(L,d^{(L)})}$	Convective outflux at $z=0$ and $z=L$	mol s^{-1}
υ	Kinematic viscosity	m^2 s^{-1}
p	Pressure	Pa
R_0	Universal gas constant	J mol^{-1} K^{-1}
$R^{(0)}_{tube}$, $R^{(L)}_{tube}$	Tube radius at $z=0$ and $z=L$	m
R^2	Coefficient of determination	dimensionless
ρ	Density	kg m^{-3}
t	Time	s, min, h
T	Temperature	K
u	Velocity	m s^{-1}
u_0	Speed of sound	m s^{-1}
x	Molar fraction	dimensionless
y_0, y_L	Pipe coordiante at $z=0$ and $z=L$	dimensionless
z	Tube coordinate	dimensionless

Appendix B

See Fig. B1.

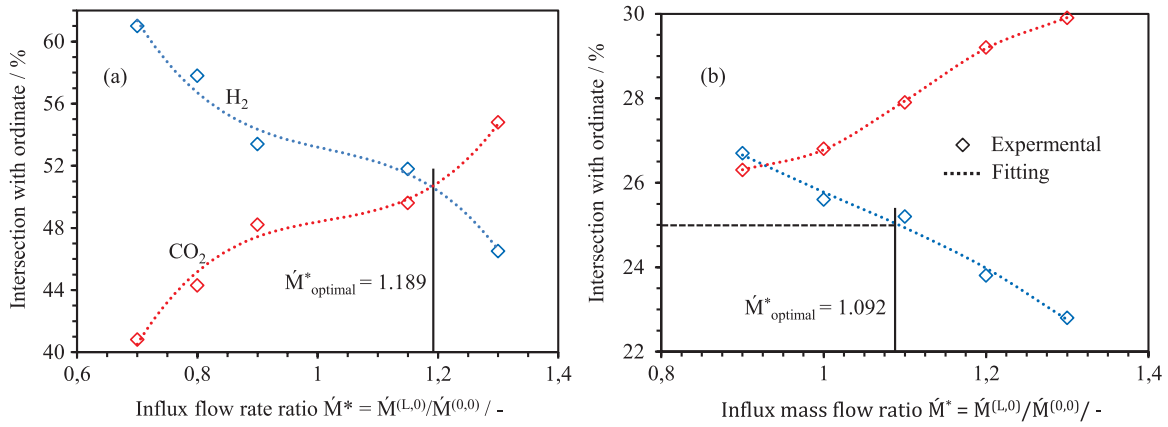

Fig. B1. (a) Determination of the optimal flow rate ratio for the binary system. The optimal flow rate ratio is taken as $\acute{M}^* = 1.189$, since third order polynominal regressions of H_2 and CO_2 molar fractions intersect and it counts: $\boldsymbol{x}_{\mathbf{H_2}} = \mathbf{x}_{\mathbf{CO_2}} \approx 50$ %, see Eq. (A2). (b) Determination of the optimal flow rate ratio for the ternary system. Third order polynomial regressions of H_2 and CO_2 molar fractions are applied. The optimal flow rate ratio is taken as $\acute{M}^* = 1.092$, since the regression curve of H_2 molar fraction, not influenced by multicomponent effects, reaches its equilibrium state at $\mathbf{x}_{\mathbf{H_2}} \approx 0.25$, see Eq. (A2). It is found graphically as the intersection of the horizontal line at $\mathbf{x}_{\mathbf{H_2}}(\acute{M}^{(\mathbf{L},\mathbf{0})} = 0) = 0.25$ with the H_2 regression curve.

Initially, the standard mass flowrate of MFC 1 at $z = 0$ ($\acute{M}^{(0,0)}$) is held constant for eight different values between 1.5 and 9 mlN min^{-1} during each experiment. The standard mass flowrate of MFC 2 at $z = L_{\text{tube}}$ ($\acute{M}^{(L,0)}$) is fixed as the product of a prefactor and the standardmass flowrate of MFC 1, to the effect that we obtain the mass flow rate ratio $\acute{M}^*$

$$\acute{M}^*=\frac{\acute{M}^{(L,0)}}{\acute{M}^{(0,0)}}. \tag{A1}$$

According to Fig. 5 the composition of the gas is analyzed with the mass spectrometer and the concentrations of the species are plotted against the standard mass flowrate of MFC 1 for the mass spectrometer at position $z = 0$ (pipe A) and against that one of MFC 2 for the case of the mass spectrometer assembled at position $z = L_{\text{tube}}$ (pipe B).

Since very low flowrates are not possible due to the lower limits of the MFCs, an extrapolating curve fitting is applied to the experimental data for each $\acute{M}^*$. The fitting model is based on the logistic function, a S-shape curve, and the molar fraction x_i versus the standard mass flowrate $\acute{M}$ is defined as

$$x_i=G\frac{1}{1+\exp\ (-Gk\acute{M})\left(\frac{G}{x_i(\acute{M}=0)}-1\right)}. \tag{A2}$$

Here, G is the barrier, k is a conversion factor and $x_i(\acute{M}=0)$ is the intersection with the ordinate axis. After the analysis of preliminary tests, the preferred parameter is $x_i(\acute{M}^{(L,0)}=0)$ during the experiments and it is varied from $0.3 \le x_i(\acute{M}^{(L,0)}=0) \le 0.7$. For each $x_i(\acute{M}^{(L,0)}=0)$, Eq. (A2) is fitted to the experimental data of $\acute{M}^*$ and the coefficient of determination is calculated. The $x_i(\acute{M}^{(L,0)}=0)$ with the highest coefficient of determination ($R^2 \to 1$) is assumed to be the best fit to the experimental data of $\acute{M}^*$.

To find the optimal mass flow rate ratio, two limiting cases are assumed. First, if the flowrate is zero on each side, only diffusion will occur and the composition in the duct will be the same on each side. For this reason, the outflux molar fraction will be determined as

$$\lim_{\acute{M}^{(0,0)}\to 0} x_i^{(0,d^{(0)})}=\lim_{\acute{M}^{(L,0)}\to 0} x_i^{(L,d^{(L)})}. \tag{A3}$$

Second, if the flowrate is infinite in each pipe, the contribution of diffusion is negligible and the composition of the outfluxes will be the same as the influxes on each side

$$\lim_{\acute{M}^{(0,0)}\to \infty} x_i^{(0,d^{(0)})}=x_i^{(0,0)},\ \lim_{\acute{M}^{(0,0)}\to \infty} x_i^{(L,d^{(L)})}=x_i^{(L,0)}. \tag{A4}$$

Consequently, $\acute{M}^*$ with the best fit for Eq. (A2) will be the optimal, experimentally determined flow rate ratio. For this reason, the intersections with the ordinate axis $x_i(\acute{M}^{(L,0)}=0)$ for the best fits are plotted against the mass flow rate ratio in the range $0.9 \le \acute{M}^* \le 1.3$ as shown in Fig. B1a for the binary system. Here we obtain $\acute{M}^* = 1.189$ for the optimal flow rate ratio.

For the ternary system we observed that regarding the fittings and their intersections with the ordinate axis, the molar fractions of CO_2 decrease delayedly with reducing flow rates compared to the increase of H_2molar fractions. Hence, the curves do not intersect on the ordinate axis at $x_{H_2}^{(L,d^{(L)})} = x_{CO_2}^{(L,d^{(L)})}=25\%$, but at higher molar fractions, $x_{H_2}^{(L,d^{(L)})}=x_{CO_2}^{(L,d^{(L)})} > 25\%$. The delayed decrease of CO_2 is assumed to be caused by multicomponent effects of N_2 (Veltzke et al., 2015; Duncan and Toor, 1962). Hence, only H_2 is used to determine the mass flow rate ratio. Again, the intersections of the H_2 and CO_2 fits with the ordinate axis $x_i(\acute{M}^{(L,0)}=0)$ are plotted against the mass flow ratio $\acute{M}^*$ in Fig. B1b.

In Fig. 8, the intersections of the CO_2 molar fraction with the axis of ordinate, $x_{CO_2}(\acute{M}^{(L,0)}=0)$, increase and those of H_2, $x_{H_2}(\acute{M}^{(L,0)}=0)$, decrease with rising influx mass flow ratio $\acute{M}^*$. Here, the optimal mass flow ratio is $\acute{M}^* = 1.092$ and given as the intersection of the horizontal line at $x_{H_2}(\acute{M}^{(L,0)}=0) = 25$ % with the regression curve of H_2. In this case, the flowrate $\acute{M}^{(L,0)}$ is zero and H_2 gas diffuses to the opposite side of the test tube until an equilibrium is reached. Since no convection and multicomponent effects occur, H_2 equilibrates to obtain a final composition of $x_{H_2} \approx 25$ % (Eq. (A2)).

Appendix C

See Tables C1–C4.

Table C1
Comparison of calculations using the analytical model according to Eq. (34) and experimental results for binary diffusion in the *uniform* tube.

Influx		Outflux molar fraction at position $z=0$						Outflux molar fraction at position $z=L$					
F(0,0)ml min^{-1}	F(L,0)ml min^{-1}	Model (dimensionless)		Experimental (dimensionless)		Deviation (%)		Model (dimensionless)		Experimental (dimensionless)		Deviation (%)	
		x_H_2	x_CO_2	x_H_2	x_CO_2	H_2	CO_2	x_H_2	x_CO_2	x_H_2	x_CO_2	H_2	CO_2
8.23	8.29	0.936	0.064	0.915	0.084	2.2	30.2	0.203	0.797	0.211	0.788	3.8	1.1
7.29	7.13	0.929	0.071	0.909	0.090	2.2	27.2	0.222	0.778	0.234	0.765	5.1	1.5
6.32	6.04	0.920	0.080	0.900	0.100	2.3	25.0	0.244	0.756	0.258	0.740	6.0	2.0
5.31	4.98	0.908	0.092	0.885	0.114	2.5	24.2	0.269	0.731	0.285	0.713	6.0	2.3
4.29	3.96	0.891	0.109	0.865	0.134	2.9	23.4	0.300	0.700	0.321	0.678	6.7	3.1
3.24	2.95	0.866	0.134	0.834	0.165	3.6	22.5	0.339	0.661	0.359	0.640	5.9	3.2
2.18	1.96	0.821	0.179	0.784	0.214	4.5	19.6	0.390	0.610	0.403	0.596	3.3	2.3
1.64	1.46	0.785	0.215	0.743	0.254	5.3	18.3	0.420	0.580	0.429	0.569	2.2	1.8

Table C2
Comparison of calculations using the analytical model according to Eq. (34) and experimental results for binary diffusion in the *conical* tube.

Influx F(0,0)ml min^{-1}	F(L,0)ml min^{-1}	Outflux molar fraction at position $z=0$ Model (dimensionless)		Experimental (dimensionless)		Deviation (%)		Outflux molar fraction at position $z=L$ Model (dimensionless)		Experimental (dimensionless)		Deviation (%)	
		x_H_2	x_CO_2	x_H_2	x_CO_2	H_2	CO_2	x_H_2	x_CO_2	x_H_2	x_CO_2	H_2	CO_2
8.23	8.29	0.913	0.087	0.935	0.065	2.4	26.0	0.247	0.753	0.192	0.808	22.5	7.4
7.29	7.13	0.905	0.095	0.930	0.070	2.8	26.8	0.267	0.733	0.214	0.786	19.7	7.2
6.32	6.04	0.894	0.106	0.922	0.077	3.2	27.2	0.289	0.711	0.240	0.760	16.9	6.9
5.31	4.98	0.879	0.121	0.912	0.088	3.7	27.5	0.314	0.686	0.271	0.728	13.6	6.2
4.29	3.96	0.859	0.141	0.897	0.102	4.5	27.7	0.344	0.656	0.305	0.695	11.3	5.9
3.24	2.95	0.828	0.172	0.874	0.125	5.5	26.9	0.379	0.621	0.351	0.649	7.6	4.6
2.18	1.96	0.779	0.221	0.834	0.165	7.0	25.3	0.423	0.577	0.406	0.594	4.1	2.9

Table C3
Comparison of calculations using the analytical model according to Eq. (35) and experimental results for ternary diffusion in the *uniform* tube.

Influx (ml min^{-1})		Outflux molar fraction at position $z=0$									Outflux molar fraction at position $z=L$								
F(0,0)	F(L,0)	Model x_i (dimensionless)			Experiment x_i (dimensionless)			Deviation (%)			Model x_i (dimensionless)			Experiment x_i (dimensionless)			Deviation (%)		
		H_2	**N_2**	**CO_2**	**H_2**	**N_2**	**CO_2**	**H_2**	**N_2**	**CO_2**	**H_2**	**N_2**	**CO_2**	**H_2**	**N_2**	**CO_2**	**H_2**	**N_2**	**CO_2**
8.77	8.92	0.448	0.538	0.014	0.430	0.557	0.013	4.1	3.5	6.3	0.087	0.470	0.443	0.095	0.478	0.426	8.9	1.7	3.8
7.34	7.28	0.441	0.543	0.016	0.423	0.560	0.017	4.0	3.1	1.5	0.099	0.466	0.435	0.106	0.476	0.417	6.8	2.3	4.2
6.35	6.22	0.434	0.547	0.019	0.417	0.562	0.020	4.0	2.8	9.0	0.109	0.463	0.428	0.115	0.475	0.409	5.4	2.7	4.5
5.33	5.17	0.426	0.552	0.022	0.408	0.566	0.025	4.0	2.5	14.2	0.121	0.459	0.419	0.126	0.474	0.399	3.9	3.2	4.9
4.29	4.12	0.414	0.559	0.027	0.396	0.570	0.033	4.3	2.1	21.2	0.136	0.456	0.408	0.139	0.473	0.387	2.2	3.9	5.4
3.24	3.08	0.398	0.567	0.035	0.380	0.576	0.043	4.6	1.7	22.9	0.155	0.452	0.393	0.156	0.474	0.369	0.5	4.9	6.2
2.17	2.05	0.375	0.576	0.050	0.355	0.583	0.062	5.2	1.2	24.1	0.180	0.449	0.372	0.178	0.478	0.342	0.7	6.5	7.9
1.63	1.54	0.359	0.561	0.080	0.337	0.585	0.077	6.2	4.3	3.7	0.196	0.462	0.342	0.192	0.483	0.324	2.1	4.5	5.4

Table C4
Comparison of calculations using the analytical model according to Eq. (34) and experimental results for ternary diffusion in the *conical* tube.

Influx (ml min^{-1})		Outflux molar fraction at position $z=0$									Outflux molar fraction at position $z=$L								
F(0,0)	F(L,0)	Model xi (dimensionless)			Experiment xi (dimensionless)			Deviation (%)			Model xi (dimensionless)			Experiment xi (dimensionless)			Deviation (%)		
		H_2	**N_2**	**CO_2**	**H_2**	**N_2**	**CO_2**	**H_2**	**N_2**	**CO_2**	**H_2**	**N_2**	**CO_2**	**H_2**	**N_2**	**CO_2**	**H_2**	**N_2**	**CO_2**
8.77	8.92	0.433	0.550	0.017	0.435	0.558	0.007	0.4	1.5	61.1	0.107	0.462	0.431	0.090	0.479	0.430	16.3	3.8	0.2
7.34	7.28	0.424	0.555	0.021	0.429	0.561	0.009	1.2	1.1	57.2	0.120	0.458	0.421	0.101	0.478	0.420	15.6	4.2	0.4
6.35	6.22	0.417	0.559	0.024	0.423	0.564	0.012	1.5	1.0	50.6	0.130	0.456	0.414	0.110	0.477	0.412	15.2	4.6	0.6
5.33	5.17	0.407	0.565	0.028	0.416	0.568	0.016	2.1	0.6	45.2	0.143	0.453	0.405	0.121	0.476	0.401	15.0	5.2	0.9
4.29	4.12	0.395	0.570	0.035	0.405	0.573	0.021	2.6	0.4	39.1	0.157	0.450	0.394	0.134	0.476	0.388	14.4	5.7	1.3
3.24	3.08	0.378	0.578	0.044	0.390	0.580	0.029	3.3	0.4	35.1	0.175	0.447	0.378	0.152	0.477	0.369	13.3	6.6	2.3
2.17	2.05	0.356	0.568	0.076	0.368	0.588	0.043	3.2	3.6	43.5	0.197	0.458	0.346	0.176	0.482	0.339	10.4	5.3	2.1

References

Bird, R.B., Stewart, W.E., Lightfoot, E.N., 2007. Transport Phenomena. Wiley, New York.

Bronskhorst High-Tech B.V., Fluidat on the Net [Online], Available: ⟨https://www.fluidat.com/default.asp⟩.

Cussler, E.L., 1997. Diffusion: Mass Transfer in Fluid Systems. Cambridge University Press, Cambridge.

Dogu, G., Dogu, T.A., 1980. General criterion to test the importance of diffusion limitations in bidisperse porous catalysts. AIChE J. 26, 287.

Dogu, T., 1998. Diffusion and reaction in catalyst pellets with bidisperse pore size distribution. Ind. Eng. Chem. Res. 37, 2158.

Duncan, J.B., Toor, H.L., 1962. An experimental study of three component gas diffusion. AIChE J. 8, 38–41.

Evans, R.B., Truitt, J., Watson, G.M., 1961. Interdiffusion of helium and argon in a large-pore graphite. J. Chem. Eng. Data 6, 522–525.

Fahien, R.W., 1983. Fundamentals of Transport Phenomena. McGraw-Hill, New York.

Falta, R.W., Javandel, I., Pruess, K., Witherspoon, P.A., 1989. Density-driven flow of gas in the unsaturated zone due to the evaporation of volatile organic-compounds. Water Resources Res. 25, 2159–2169.

Falta, R.W., Pruess, K., Javandel, I., Witherspoon, P.A., 1992. Numerical modeling of steam injection for the removal of nonaqueous phase liquids from the subsurface. 1. Numerical formulation. Water Resources Res. 28, 433–449.

Farr, J.M., 1993. Advective-Diffusive Gaseous Transport in Porous Media: The Molecular Diffusion Regime (Dissertation). Department of Agricultural and Chemical Engineering, Colorado State University, Colorado.

Fick A., 1855. Über Diffusion, Poggendorff's Annalen der Physik, vol. 170, pp. 59–86.

Graham T., 1883. On the Law of the Diffusion of Gases, The London and Edinburgh Philosophical Magazine and Journal of Science, 2. Aufl.

Graur, I., Veltzke, T., Méolans, J.G., Ho, M.T., Thöming, J., 2015. The gas flow diode effect: theoretical and experimental analysis of moderately rarefied gas flows through a microchannel with varying cross section. Microfluid. Nanofluidics 18, 391–402.

Hassanizadeh, M., Gray, W.G., 1979. General conservation equations for multi-phase systems: 2. Mass, momenta, energy, and entropy equations. Adv. Water Resources 2, 191–203.

Loewenberg, M., 1994. Diffusion-controlled, heterogeneous reaction in a material with a bimodal pore size distribution. J. Chem. Phys. 100, 7580.
Pollock, D.W., 1986. Simulation of fluid-flow and energy-transport processes associated with high-level radioactive-waste disposal in unsaturated alluvium. Water Resources Res. 22, 765–775.
Soukup, K., Schneider, P., Solcova, O., 2008. Comparison of Wicke–Kallenbach and Graham's diffusion cells for obtaining transport characteristics of porous solids. Chem. Eng. Sci. 63, 1003–1011.
Taylor, R., Krishna, R., 1993. Multicomponent Mass Transfer. John Wiley and Sons, New York.
Veltzke, T., Kiewidt, L., Thöming, J., 2015. Multicomponent gas diffusion in non-uniform tubes. AIChE J. 61, 1404–1412.
Wang, G., Coppens, M.-O., 2008. Calculation of the optimal macropore size in nanoporous catalysts and its application to DeNOx catalysis. Ind. Eng. Chem. Res. 47, 3847–3855.
Wicke, E., Kallenbach, R., 1941. Die Oberflächendiffusion von Kohlendioxyd in aktiven Kohlen. Kolloid Z. 97, 135–151.